CONTENTS

	Page	
SUMMARY	1	1/A6
INTRODUCTION	2	1/A7
SYMBOLS	3	1/A8
THE MATHEMATICAL ANALYSIS	5	1/A10
Summary of the Computational Procedure	5	1/A10
Vorticity Transport Equations	6	1/A11
THE DEVELOPMENT OF THE FLOW	8	1/A13
The Progressing in Time	8	1/A13
The Biot-Savart Law	8	1/A13
Development of the Vorticity	9	1/A14
Intensity of the New Vorticity	10	1/B1
DETAILS OF THE SOLUTION PROCEDURE	12	1/B3
The Vorticity Transport Equations	12	1/B3
Computation of the Additional Vorticity	12	1/B3
CONCLUDING REMARKS	13	1/B4
APPENDIX A - The Vorticity Transport Equations	17	1/B8
APPENDIX B - The Velocity Field	21	1/B12
APPENDIX C - The Vortex Sheet	23	1/B14
APPENDIX D - Representation of the Wing Boundary	25	1/C2
APPENDIX E - Representation of the Two-Dimensional Fluid Region	28	1/C5
REFERENCES	34	1/C11

ILLUSTRATIONS

Figure		Page	
1	Sequences of computations in the computational procedure	15	1/B6
D1	The curvilinear element after Argyris and Scharpf . . .	25	1/C2
E1	Illustration of the finite-element mesh	28	1/C5
E2	The isoparametric quadrilateral finite-element	30	1/C7
E3	The isoparametric triangular finite-element	32	1/C9

NASI.26:2995

JUN 16 1978

NASA Contractor Report 2995

COMPLETED
ORIGINAL

Computational Flow Development for Unsteady Viscous Flows

Foundation of the Numerical Method

Theodore Bratanow and Thomas Spehert

GRANT NGR-50-007-001
MAY 1978

NASA

41

NASA 26 2995

NASA Contractor Report 2995

Computational Flow Development for Unsteady Viscous Flows

Foundation of the Numerical Method

Theodore Bratanow and Thomas Spehert
University of Wisconsin-Milwaukee
Milwaukee, Wisconsin

Prepared for
Langley Research Center
under Grant NGR-50-007-001

National Aeronautics
and Space Administration

Scientific and Technical
Information Office

1978

BLANK PAGE

SUMMARY

A procedure is presented for effective consideration of viscous effects in computational development of high Reynolds number flows. The procedure is based on the interpretation of the Navier-Stokes equations as vorticity transport equations. The physics of the flow has been represented in a form suitable for numerical analysis. Lighthill's concept for flow development for computational purposes has been adapted. The vorticity transport equations were cast in a form convenient for computation. A statement for these equations was written using the method of weighted residuals and applying the Galerkin criterion. An integral representation of the induced velocity was applied on the basis of the Biot-Savart law. The numerical procedure developed by Hess and Smith and then refined by Argyris and Scharpf was used in computing vortex sheets over curved wing surfaces. Distribution of new vorticity, produced at wing surfaces over small computational time intervals, was assumed to be confined to a thin region around the wing surfaces. This report presents thus the foundation and components of the numerical method. A following report will present the details of the implementation of the computational procedure.

INTRODUCTION

Theoretical treatment of unsteady viscous flow effects and extension of the Reynolds number range are of primary concern as well as having great urgency from an application point of view (ref. 1). For higher Reynolds number flows, the effect of viscosity becomes increasingly confined to narrow regions of the wing surface and laminar flows break down and become turbulent (ref. 2). The treatment of viscous effects and high Reynolds number flows is still not presented well in theoretical analyses (ref. 1).

The Navier-Stokes equations, as the mathematical model of unsteady viscous flow, contain all features needed for the solution of the problem. Advances, however, in establishing practical, meaningful relations between vorticity development and diffusion have been slow. Ingenious schemes have been applied in seeking to obtain solutions of the Navier-Stokes equations. Solutions of this kind have thus far been confined to flows of relatively low Reynolds numbers, and they are still inadequate for actual aeronautical applications (ref. 1). By applying suitable discretization and computational procedures, attempts have been made to extend the solutions to higher Reynolds numbers (ref. 3). The obtained results with viscous flows of moderately high Reynolds numbers have been achieved through a long struggle with mathematics, fluid dynamics, and tedious numerical analyses. For instance, presented data and computer plots, although giving a blurred picture of viscous flow patterns, have been of genuine interest (ref. 4).

Since the finite-element methods are well suited for theoretical treatment of unsteady viscous flows past bodies of complex geometry, and since configurations of finite-element meshes can be suitably clustered in regions of significant changes in the flow patterns, there has been a vivid interest and much work done in this area (ref. 5). There is expectation that finite-element methods will provide a solid numerical foundation for treatment of high Reynolds number flows. The purpose of this report has been the presentation of such a foundation.

It appears that four different formulations have been commonly applied in conjunction with discretization methods: the formulations with respect to stream function, stream function and vorticity, velocity and pressure (ref. 6), and the Lighthill vorticity-velocity concept of flow development for computational purposes (ref. 7). Interpretations of the Lighthill concept, using the finite-difference method, have been presented by Payne (ref. 8) and by Schmall and Kinney (ref. 9), as well as in conjunction with an integro-differential formulation by Wu (refs. 10 and 11).

The authors are deeply grateful to Dr. G.M.L. Gladwell, Professor, University of Waterloo, Waterloo, Ontario, Canada, and to Dr. Ch. Hirsch, Professor, University of Brussels, Brussels, Belgium, for the kindly provided assistance and specialized expertise for the research toward this report. Acknowledged gratefully is also the support from the NATO grant No: 1264 through which it was possible for Professor Hirsch to participate in the research.

SYMBOLS

A	fluid region, m^2
dA	fluid element containing vorticity $\omega(t+\delta t)$, m^2
c	wing boundary
g	number of integration points
L_j	Lagrangian interpolation polynomials
ℓ_1, ℓ_2, ℓ_3	area coordinates
M^k	weighting functions
m	number of element nodes
N_i	nodal shape functions
n	unit vector normal to the wing surface
q_k	parameters
$\underline{r}$	position vector relative to dA or dS respectively; also a distance, m
dS	element of a vortex sheet
t	time, sec
$\underline{t}$	unit vector tangent to the wing surface
δt	subsequent time-step, sec
$\underline{U}_\infty$	uniform onset velocity of the fluid in region A; constant in time, m/sec
u_j, v_j	nodal values of velocity, m/sec
$\underline{v}(t)$	no-slip velocity, m/sec
$\underline{v}(t+\delta t)$	velocity which does not satisfy the no-slip condition at the beginning of iteration, m/sec
$\underline{v}_\gamma(t+\delta t)$	induced velocity due to vortex sheet, m/sec
$\underline{v}_\omega$	induced velocity at a point in the fluid, m/sec
$\underline{v}_{\omega^*}$	additional induced velocity, m/sec
W	a function
w_k	weights
x,y,z	Cartesian coordinates
γ_i	nodal values of vortex sheet intensity, m/sec
$\gamma(t+\delta t)$	vortex sheet, m/sec

ν	kinematic viscosity, m^2/sec
ξ,η	element local coordinates
ρ	uniform density, kg/m^3
ω_j	vorticity at a finite-element node, 1/sec
$\omega(t)$	vorticity, 1/sec
ω^*	additional vorticity during time δt, 1/sec
ω_*^k	undetermined parameters

Matrix Symbols

[A]	convection coefficient matrix
$\{B\}^e$	finite-element vector containing wing boundary conditions
[C]	vortex sheet coefficient matrix
{F}	a vector
$\{\gamma\}$	unknown vector
[J]	Jacobian
[m]	mass matrix
[S]	diffusion matrix

Subscripts

e	over a finite-element
f.e.	finite-element
i	element node
x,y	partial derivatives with respect to x and y respectively

THE MATHEMATICAL ANALYSIS

In unsteady viscous flows around wing boundaries, there exists a very narrow region in which gradients of flow field variables and influence of viscous forces are very large. At higher Reynolds number flows, and flows around oscillating wings in particular, the situation is even more complicated. The proper solution requires consideration of the entire flow field around the wing. There is a need of a reasonably efficient and accurate method for treatment of such flows. In principle, the time-dependent Navier-Stokes equations, as the mathematical model, contain all the features needed for the solution of the laminar and turbulent aspects of the flow. The interpretation of these equations as vorticity transport equations extends Helmholtz's equations to viscous flows (refs. 12 and 13).

Numerical methods of solution appear to provide the only hope of producing quantitative results. The procedure described below offers the foundation of such an approach. For reliable results about the viscous region around the wing, the Lighthill concept of flow development for computational purposes (ref. 7) has been adapted here. It is thus important to provide for the proper inclusion of vorticity in the numerical analysis of the field variables of the complete flow.

Summary of the Computational Procedure

The vorticity transport equations were cast in a form convenient for computation (refs. 14 and 15). The computation is considered unsteady in the sense of being suitable for time-stepped solutions. A statement for these equations was written using the method of weighted residuals and applying the Galerkin criterion (see appendix A). From the discretized form of the equations, finite-element equations were assembled and summed over all elements forming thus the global system of equations for the complete flow region. The discretization in finite-element form of the vorticity transport equations resulted in a system of differential equations with respect to time. These equations can be solved with respect to the time variable using a finite difference technique (ref. 5). Finite-elements in the fluid region contain vorticity, since vorticity will be found only in that portion of the fluid region which is discretized by finite-elements.

An integral representation of the induced velocity at finite-element nodes due to the vorticity distribution was applied on the basis of the Biot-Savart law. Details are shown in appendix B. The numerical procedure developed by Hess and Smith (ref. 16) and then refined by Argyris and Scharpf (ref. 17) was used in computing vortex sheets over the curved wing surface (see appendix C). The refinement introduced by Argyris and Scharpf involved curvilinear elements, in place of the plane elements used by Hess and Smith (see appendix D). A Hermitian interpolation model was used to approximate the geometry of curvilinear elements between nodes defining the elements. A Lagrangian interpolation model was used to describe vortex sheet intensity over finite-elements. Two types of finite-elements were applied in representing the flow region under investigation: isoparametric triangular and isoparametric quadrilateral finite-elements. Surrounding the curved wing surface are quadrilateral finite-

elements, with the remainder of the fluid region divided into triangular finite-elements of varying sizes, becoming smaller and smaller near the wing surface. Quadratic shape-functions were utilized for both isoparametric triangular and isoparametric quadrilateral finite-elements. Details are shown in appendix E.

Vorticity transport equations - In three-dimensional form the vorticity transport equations can be written in fixed coordinates (ref. 13) as

$$\frac{\partial \underline{\omega}}{\partial t} = (\underline{\omega}\cdot\underline{\nabla})\underline{v} - (\underline{v}\cdot\underline{\nabla})\underline{\omega} + \nu\nabla^2\underline{\omega} \tag{1}$$

In the case of two-dimensional flow $(\underline{\omega}\cdot\text{grad})\underline{v} = 0$ and $\frac{d\underline{\omega}}{dt} = \nu\nabla^2\underline{\omega}$, i.e., the total variation of vorticity is equal to the rate of dissipation of vorticity through friction (ref. 12). The two-dimensional form of equation (1) is

$$\frac{\partial \omega}{\partial t} = -(\underline{v}\cdot\underline{\nabla})\omega + \nu\nabla^2\omega \tag{2}$$

whereby only convection and viscous conduction take place (ref. 15). Equation (2) is discretized in space using the finite-element method. Over each finite-element, the vorticity and velocity components are approximated by their nodal values, ω_j, u_j, and v_j, and by the nodal shape functions N_j. Then

$$\omega(\xi,\eta) = \sum_{j=1}^{m} N_j(\xi,\eta)\omega_j = \{N\}^t\{\omega\}^e \tag{3}$$

$$u(\xi,\eta) = \sum_{j=1}^{m} N_j(\xi,\eta)u_j = \{N\}^t\{u\}^e \tag{4}$$

$$v(\xi,\eta) = \sum_{j=1}^{m} N_j(\xi,\eta)v_j = \{N\}^t\{v\}^e \tag{5}$$

The finite-element is defined here by m nodes. The element shape functions are expressed in terms of the local coordinates (ξ,η), which range between unity and zero within the finite-element. The coordinate η will be chosen to be normal to the wing boundary. The weighted residual statement for the vorticity transport equations is written as

$$\int_A N_i\left\{ \frac{\partial \omega}{\partial t} + \frac{\partial}{\partial x}(u\omega) + \frac{\partial}{\partial y}(v\omega) - \nu\left(\frac{\partial^2\omega}{\partial x^2} + \frac{\partial^2\omega}{\partial y^2} \right) \right\} dA = 0 \tag{6}$$

In equation (6) the weighting functions of the method of weighted residuals have been set equal to the finite-element shape functions, N_i, in accordance with the Galerkin criterion. Applying an integration by parts to the second-order viscous terms, the expression becomes

$$\int_A \left[N_i \left\{\frac{\partial \omega}{\partial t} + \frac{\partial}{\partial x}(u\omega) + \frac{\partial}{\partial y}(v\omega)\right\} + \nu \left\{\frac{\partial N_i}{\partial x}\frac{\partial \omega}{\partial x} + \frac{\partial N_i}{\partial y}\frac{\partial \omega}{\partial y}\right\}\right] dA \tag{7}$$

$$- \nu \oint_c N \frac{\partial \omega}{\partial \eta} dc = 0$$

The expression in equation (7) is discretized in finite-element form. Over each finite-element, the vorticity transport equations can be written in matrix form as

$$[m]^e \left\{\frac{\partial \omega}{\partial t}\right\}^e = [A]^e \{\omega\}^e + [S]^e \{\omega\}^e + \{B\}^e \tag{8}$$

where the element matrices and the vector, after substitution of equations (3), (4), and (5) into equation (7) are defined as follows:

$$[m]^e = \int_A \{N\}\{N\}^t \, dA \tag{9}$$

$$[A]^e = - \int_A \left[\{N\}\{u\}^t \{N\}\{N_x\}^t + \{N\}\{v\}^t \{N\}\{N_y\}^t\right] dA \tag{10}$$

$$[S]^e = - \nu \int_A \left[\{N_x\}\{N_x\}^t + \{N_y\}\{N_y\}^t\right] dA \tag{11}$$

Here equations (9-11) are respectively the element mass matrix and the convection and diffusion matrices. Matrix [A] is an unsymmetric matrix, representing the nonlinear convective terms in the vorticity transport equations. It is a function of the no-slip velocity field $\underline{v}(t)$ corresponding to the no-slip condition. Partial derivatives with respect to x and y are indicated by subscripts x or y respectively. The finite-element vector $\{B\}^e$, containing the wing boundary conditions, is written as

$$\{B\}^e = \nu \oint_c \{N\} \left\{\frac{\partial \omega}{\partial \eta}\right\} dc = [B]^e \{\omega\}^e \tag{12}$$

It results from the integration by parts. Here

$$[B]^e = \nu \oint_c \{N\}\{N_n\}^t \, dc$$

The element matrix [B] is constant in time and is computed only once for each element and then stored. The contour integral is not evaluated on the outer boundary since the region covered by finite-elements contains all the vorticity in the flow and therefore ω is identically zero at the outer boundary.

The numerical integration used to evaluate the integrals of equations

(9-12) is carried out in the local coordinate system of the finite-element, where

$$dx\,dy = \det.\,[J]\,d\xi\,d\eta \tag{13}$$

is used to transform the region with respect to which the integration is carried out. The vorticity transport equation, in the form of equation (8), is then solved in time over the subsequent time-step δt using a finite-difference technique to obtain a new distribution of the vorticity at time $t+\delta t$, which, in general, is different from that vorticity distribution which is known at time t.

THE DEVELOPMENT OF THE FLOW

The manner of progressing from the velocity and vorticity distribution at an initial time instant t to the vorticity and velocity distribution of a subsequent time instant $(t+\delta t)$ will now be outlined. Consider, however, that some time t has elapsed since the fluid was set in motion past the wing.

The progressing in time - At time instant t, the flow variables, $\underline{v}(t)$ and $\omega(t)$, are assumed to be known and that the no-slip velocity condition is satisfied on the wing boundary c. That is, in solving equation (8) the no-slip velocity field $\underline{v}(t)$ has to be used. Since vorticity is a measure of the angular momentum of the fluid particles in motion, in the two-dimensional case the vorticity ω has a single component, perpendicular to the plane of motion x and y.

During the subsequent time interval δt, the flow variables $\underline{v}(t)$ and $\omega(t)$ are advanced to their new values at $t+\delta t$. Through convection and diffusion, the known vorticity $\omega(t)$ is redistributed, while during the same time interval, δt, new vorticity is diffusing into the fluid from the wing boundary c in such a manner that the no-slip condition is satisfied.

The Biot-Savart law - Consider first the redistribution of the known vorticity $\omega(t)$ through convection and diffusion. By solving equation (8), the redistribution of $\omega(t)$ at $t+\delta t$ is given as $\omega(t+\delta t)$. Then the induced velocity, which coexists along with the vorticity $\omega(t+\delta t)$, is given by the Biot-Savart law as

$$\underline{v}_{\omega}(t+\delta t) = \frac{1}{2\pi}\int_{A}\frac{\underline{\omega}(t+\delta t)\times\underline{r}}{|\underline{r}|^{2}}\,dA \tag{14}$$

where the integration is over the whole region of the vorticity distribution. Here $\underline{r}$ is a position vector relative to the fluid element dA containing vorticity $\omega(t+\delta t)$.

Conversely, if $\underline{v}_{\omega}(t+\delta t)$ is the induced velocity at a point in the fluid, the vorticity at that point is by definition

$$\underline{\omega}(t+\delta t) = \underline{\nabla}\times\underline{v}_{\omega}(t+\delta t) \tag{15}$$

Here, $\underline{v}_{\omega}(t+\delta t)$ is computed by numerically integrating equation (14) over each finite-element containing vorticity and summing their individual contributions.

Development of the vorticity - In general, the induced velocity $\underline{v}_{\omega}(t+\delta t)$, resulting from the vorticity as obtained from equation (8), has a non-zero slip component at the wing boundary. Therefore, the velocity $\underline{v}(t+\delta t)$ does not, in general, satisfy the no-slip boundary condition on the wing surface at the beginning of the iteration process. The difference from the no-slip condition can be attributed to some additional vorticity $\omega^*(t+\delta t)$, produced at the wing surface over the time step δt but which was not included when the induced velocity was computed, i.e.,

$$\omega(t+\delta t) + \omega^*(t+\delta t) = \underline{\nabla} \times \underline{v}_{\omega}(t+\delta t) + \underline{\nabla} \times \underline{v}_{\omega^*}(t+\delta t)$$

Accordingly, any existing velocity field can be regarded as containing two induced velocity vectors, $\underline{v}_{\omega}(t+\delta t)$ and $\underline{v}_{\omega^*}(t+\delta t)$. The complete velocity field at $t+\delta t$, at any point in the fluid, can be defined (refs. 7, 18, and 19) as

$$\underline{v}(t+\delta t) = \underline{v}_{\omega}(t+\delta t) + \underline{v}_{\omega^*}(t+\delta t) + \underline{U}_{\infty} \tag{16}$$

The velocity $\underline{v}(t+\delta t)$, defined by equation (16), should satisfy the no-slip condition at the wing surface. The induced velocity $\underline{v}_{\omega}(t+\delta t)$, obtained from viscous considerations, is unequal to zero at the wing surface. It is important to consider that in the framework of the concept of computational flow development, used in obtaining the solution for the flow by numerical means, we simulate the flow of vorticity in the given unsteady viscous flow by introducing elements of irrotational flow. The additional induced velocity $\underline{v}_{\omega^*}(t+\delta t)$, although calculated from irrotational flow considerations, is a viscous effect, and it is rotational by definition. It is also unequal to zero at the wing surface.

Consider now the resulting tangential velocity at the wing surface (ref. 7), before the new vorticity $\omega^*(t+\delta t)$ was accounted for. Since it may not satisfy the no-slip condition there, it appears that just enough new vorticity $\omega^*(t+\delta t)$ must have been diffused at the wing surface during the time interval δt, that the sum of the tangential components of the induced velocities due to $\omega(t+\delta t)$ and $\omega^*(t+\delta t)$ and the onset velocity will lead to zero slip. Correspondingly, equation (16) may be rewritten for the tangential components of the involved velocities on the wing surface. Upon rearranging the resulting equation one obtains

$$\underline{t} \cdot \underline{v}_{\omega^*}(t+\delta t) = - \underline{t} \cdot [\underline{v}_{\omega}(t+\delta t) + \underline{U}_{\infty}] \tag{17}$$

In sum, given the vorticity $\omega(t+\delta t)$ from the solution of equation (8), the induced velocity $\underline{v}_{\omega}(t+\delta t)$ and the velocity $\underline{v}(t+\delta t)$ can be determined from equation (16). The velocity $\underline{v}(t+\delta t)$, however, may not satisfy the no-slip condition on the wing surface c. Therefore, an additional distribution

of vorticity $\omega^*(t+\delta t)$ must be combined with the existing vorticity distribution $\omega(t+\delta t)$. The induced velocity $\underline{v}_\omega(t+\delta t)$ can be regarded also as a perturbation velocity (refs. 18 and 19).

Intensity of the new vorticity - As iteration for time-step $t+\delta t$ begins, the tangential components of velocity $\underline{v}(t+\delta t)$ at the wing surface may be unequal to zero. There exists then a discontinuity in the tangential velocity component at the wing surface, equal to the difference between the no-slip velocity and the velocity component $\underline{t}\cdot\underline{v}(t+\delta t)$. By definition, a surface across which tangential velocity changes abruptly is a vortex sheet (ref. 18). The concept of a vortex sheet is introduced now as an approximation, allowing the calculation of the additional vorticity ω^*. Following reference 18, with the induced velocity $\underline{v}_\gamma(t+\delta t)$ due to the vortex sheet $\gamma(t+\delta t)$, the velocity at a point P in the fluid can be written now as

$$\underline{v}^P(t+\delta t) = \underline{v}^P{}_\omega(t+\delta t) + \underline{v}^P{}_\gamma(t+\delta t) + \underline{U}_\infty \tag{18}$$

Following the derivation of the vortex sheet (ref. 18), the induced velocity due to the vortex sheet at a point I, just outside the wing surface, and the velocity at a point O, just inside the wing surface, may be written as

$$\underline{v}^I_\gamma(t+\delta t) = \underline{v}^*_\gamma(t+\delta t) + \frac{1}{2}\,\underline{\gamma}(t+\delta t) \times \underline{n} \tag{19}$$

and

$$\underline{v}^O_\gamma(t+\delta t) = \underline{v}^*_\gamma(t+\delta t) - \frac{1}{2}\,\underline{\gamma}(t+\delta t) \times \underline{n} \tag{20}$$

respectively. Since a straight element of vortex sheet dS cannot induce velocity at its centroid (ref. 18), the velocity $\underline{v}^*_\gamma(t+\delta t)$ is the velocity induced at its centroid by the rest of the vortex sheet, excluding the infinitesimal element dS. Moreover, the second terms on the right-hand side of equations (19) and (20) are the velocities induced at points I and O respectively by the element dS (ref. 18).

If a general point P is now identified as point O, equation (20) may be substituted into equation (18) as

$$\underline{v}^O(t+\delta t) = \underline{v}^O_\omega(t+\delta t) + \underline{v}^*_\gamma(t+\delta t) - \frac{1}{2}\,\underline{\gamma}(t+\delta t) \times \underline{n} + \underline{U}_\infty \tag{21}$$

Here $\underline{n}$ is the unit vector normal to the wing surface. Furthermore, by the above definition of the vortex sheet, the velocity at point O is set equal to the no-slip velocity,

$$\underline{v}^O(t+\delta t) = 0 = \underline{v}^O_\omega(t+\delta t) + \underline{v}^*_\gamma(t+\delta t) - \frac{1}{2}\,\underline{\gamma}(t+\delta t) \times \underline{n} + \underline{U}_\infty \tag{22}$$

Taking the tangent component of equation (22) and rearranging

$$\underline{t} \cdot \underline{v}^*_{\gamma}(t+\delta t) - \frac{1}{2}\gamma(t+\delta t) = -\underline{t} \cdot (\underline{U}_\infty + \underline{v}^0_{\omega}(t+\delta t)) \tag{23}$$

The velocity $\underline{v}^*_{\gamma}(t+\delta t)$ has been given (ref. 18) as

$$\underline{v}^*_{\gamma}(t+\delta t) = \frac{1}{2\pi}\int_S \frac{\underline{\gamma}(t+\delta t) \times \underline{r}}{|\underline{r}|^2}\, dS \tag{24}$$

which is the two-dimensional form of the Biot-Savart induction law for vortex sheets. Substituting equation (24) into equation (23)

$$\underline{t} \cdot \frac{1}{2\pi}\int_S \frac{\underline{\gamma}(t+\delta t) \times \underline{r}}{|\underline{r}|^2}\, dS - \frac{1}{2}\gamma(t+\delta t) = -\underline{t} \cdot [\underline{v}^0_{\omega}(t+\delta t) + \underline{U}_\infty] \tag{25}$$

Equation (25) is solved to obtain the vortex sheet. The integration is carried out over the wing boundary (ref. 18). The amount of new vorticity $\omega^*(t+\delta t)$, diffusing from the wing surface during the time interval δt, is found using the vortex sheet $\gamma(t+\delta t)$. A sufficient amount of new vorticity is created close to the wing boundary such that when combined with the existing vorticity $\omega(t+\delta t)$, the no-slip condition is insured. This condition, explained by Lighthill (ref. 7), insuring that the velocity normal to the airfoil surface will be zero, is expressed analytically here as follows

$$-\nu\int_t^{t+\delta t} \frac{\partial \omega}{\partial \eta}\, dt = \gamma(t+\delta t) \tag{26}$$

Nearly similar interpretations of this condition have been expressed analytically in references (9-11). Since diffusion of vorticity from a vortex sheet can be considered as a time-dependent problem, the distribution of new vorticity $\omega^*(t+\delta t)$ in the fluid could have been carried out using the finite-element vorticity transport program described previously. Since the process is iterative, it is carried out until the velocities around the wing are equal to zero for a given numerical accuracy. However, in this report an alternative approach will be used.

When it can be assumed that diffusion dominates only the vorticity $\omega^*(t+\delta t)$ over convection near the wing surface and not the vorticity $\omega(t+\delta t)$ and provided that the time-step is sufficiently small (ref. 7), the new vorticity $\omega^*(t+\delta t)$ becomes (ref. 15)

$$\omega^*(t+\delta t) = \frac{\gamma(t+\delta t)}{2}\, e^{\frac{-(\underline{n}\cdot\underline{r})^2}{4\nu\delta t}} \{\pi\nu\delta t\}^{-\frac{1}{2}} \tag{27}$$

Thus, included in equation (27) is the idea that at time $t+\delta t$, the vorticity $\omega^*(t+\delta t)$ on the left-side of the equation and the vortex sheet $\gamma(t+\delta t)$, on the right-hand side, occur simultaneously. The range of validity of equation (27) is confined to the region near the surface where viscous effects are much

larger than the vorticity convection (i.e., a computational thickness, y, much smaller than the boundary layer thickness, δ) and for times when the time derivative of diffusion is much larger than the convection of vorticity (i.e., when $U_\infty \delta t$ is much smaller than the chord multiplied by δ/y).

DETAILS OF THE SOLUTION PROCEDURE

The Vorticity Transport Equations

The details of the implementation of the solution of the vorticity transport equations, in the form of the discretized equation (8), can be summarized as follows:

a) the global mass matrix [m] is constant in time for a given finite-element mesh. It is assembled and stored in a symmetric band-storage mode at the beginning of the numerical procedure. This matrix is computed using numerical integration and then decomposed into equivalent lower and upper triangular matrices using Cholesky decomposition.

b) the time rate of change of vorticity vector $\{\frac{\partial \omega}{\partial t}\}$ is obtained using a finite-difference scheme; the initial procedure involved the Euler method with later use of the trapezoidal method and the fractional-step method.

c) the finite-element convection coefficient matrix [A] is dependent on time due to the velocity terms and must be evaluated using numerical integration each time the vorticity transport equations are solved.

d) the finite-element diffusion coefficient matrix [S] is constant in time. It is computed using numerical integration at the beginning of the computational procedure and then stored.

e) the matrix [B] is assembled for the wing boundary finite-elements only and is evaluated using numerical integration; it is also constant in time and stored at the beginning of the computational procedure.

Computation of the Additional Vorticity

The additional vorticity can be distributed using the finite-element vorticity transport program or the solution due to Lighthill's approximation, equation (27). The first approach can easily be implemented in the computer code. Hence, in what follows in this report, only the way of applying equation (27) will be described. Assumptions can be made that the distribution of new vorticity $\omega^*(t+\delta t)$, produced at the wing surface over a small time-interval δt, is confined to a thin region around the wing, and that it is dominated by diffusion.

The distribution of new vorticity determined using Lighthill's approximation, as expressed by equation (27), is proportional to the vortex sheet. A

vortex sheet may be computed from equation (25). The second term on the left-hand side of equation (25) indicates that the singularity has been properly considered. The form of the right-hand sides of both equations (17) and (25) is of interest. Accordingly, the right-hand side of equation (25) is the negative of the resulting slip velocity $\underline{v}_t(t+\delta t)$ at a point of the velocity field $\underline{v}(t+\delta t)$. This slip velocity has been defined (ref. 18) as a discontinuity in the tangential component of the velocity at the wing surface.

Equation (25) is solved numerically at a finite number of points on the wing surface. The vortex sheet $\gamma(t+\delta t)$ is described by these finite number of points and suitable interpolation functions (refs. 16 and 17). The integral in equation (25) is evaluated using a Gauss-Legendre quadrature and assembled for all nodes on the wing surface. The resulting system of equations is solved for vortex sheet $\gamma(t+\delta t)$ using a LU-decomposition. Once the vortex sheet has been computed, the distribution of additional vorticity is obtained. As it will be shown in the follow-up of this report, the actual computation of the additional vorticity may be confined to only the nodes of the first few layers of finite-elements around the wing.

At time $t+\delta t$, the new vorticity $\omega^*(t+\delta t)$ is combined with the previously computed vorticity $\omega(t+\delta t)$, with the result becoming a new estimate of the existing vorticity $\omega(t+\delta t)$ at time $t+\delta t$ or

$$\omega(t+\delta t) \leftarrow \omega(t+\delta t) + \omega^*(t+\delta t) \tag{28}$$

Equation (28) is evaluated at all finite-element nodes where the new vorticity $\omega^*(t+\delta t)$ was computed.

The new estimate for the existing vorticity $\omega(t+\delta t)$ is then used to recalculate the velocity $\underline{v}(t+\delta t)$ from equation (16). This velocity should satisfy the no-slip condition at the wing boundary. However, it may not, since the additional vorticity distribution $\omega^*(t+\delta t)$ is only an estimate based on the calculated value of the vortex sheet $\gamma(t+\delta t)$. Thus, if it does not, equation (25) can be solved again for a new vortex sheet $\gamma(t+\delta t)$, with the subsequent solutions of equations (27) and (28) giving still another estimate of the existing vorticity $\omega(t+\delta t)$ at time $t+\delta t$. Equations (25), (27), and (28) may be iterated in this manner until a sufficient amount of new vorticity $\omega^*(t+\delta t)$ is combined with the existing vorticity $\omega(t+\delta t)$ to enforce the no-slip condition at the wing boundary. Once the no-slip condition on the wing boundary is satisfied, the solution is complete and the computational procedure may be extended over the next small time-step, $t+\delta t$; starting with the solution of the vorticity transport equations. Figure (1) illustrates the main sequences of computations in the computational procedure.

CONCLUDING REMARKS AND RECOMMENDATIONS

The presented procedure offers an approach toward effective representation of viscous effects in the computational development of high Reynolds number flows. Efforts were made to represent the physics of the flow in a form suitable for numerical analysis, to contain the features needed for the

solution, and to optimize codes to reduce computer costs. Since finite-element methods are considered as computationally effective, it is expected that they will facilitate extending not only the range of Reynolds numbers of practical applications, but they hold promise for good results from three-dimensional analyses.

The numerical difficulties increase as the Reynolds numbers increase; analytical difficulties adversely affecting accuracy. Computer runs were made to test the range of application of the program and the accuracy of the results for higher Reynolds numbers. These tests have required a considerable amount of computer execution times. Portions of the program need significant optimization in order to reduce computer cost. The computation, for instance, of the induced velocity from the Biot-Savart law still involves a large portion of the computer time for a time-step. Significant instabilities occur in the numerical integration which are related to the size of the time-step of integration. Integration and computational techniques have been employed in the program with the objective of increasing the integration time-step. It is expected that the implementation of the fractional-step method will further reduce computer execution times. The numerical treatment of the wake region requires the application of the correct boundary conditions at the downstream end of the finite-element gridwork. It is thus necessary that these conditions account for the propagation of vorticity over the finite-element gridwork.

Particularly promising, for instance, is the Boundary-Element Concept which was developed just recently as a refinement in the field of discretization techniques. It has also been necessary to determine how the numerical results simulate the actual flow at comparable Reynolds numbers. There is available only a very limited amount of suitable experimental results for comparisons. However, the prospects for such comparisons have improved since interest in suitable experimental research has also increased.

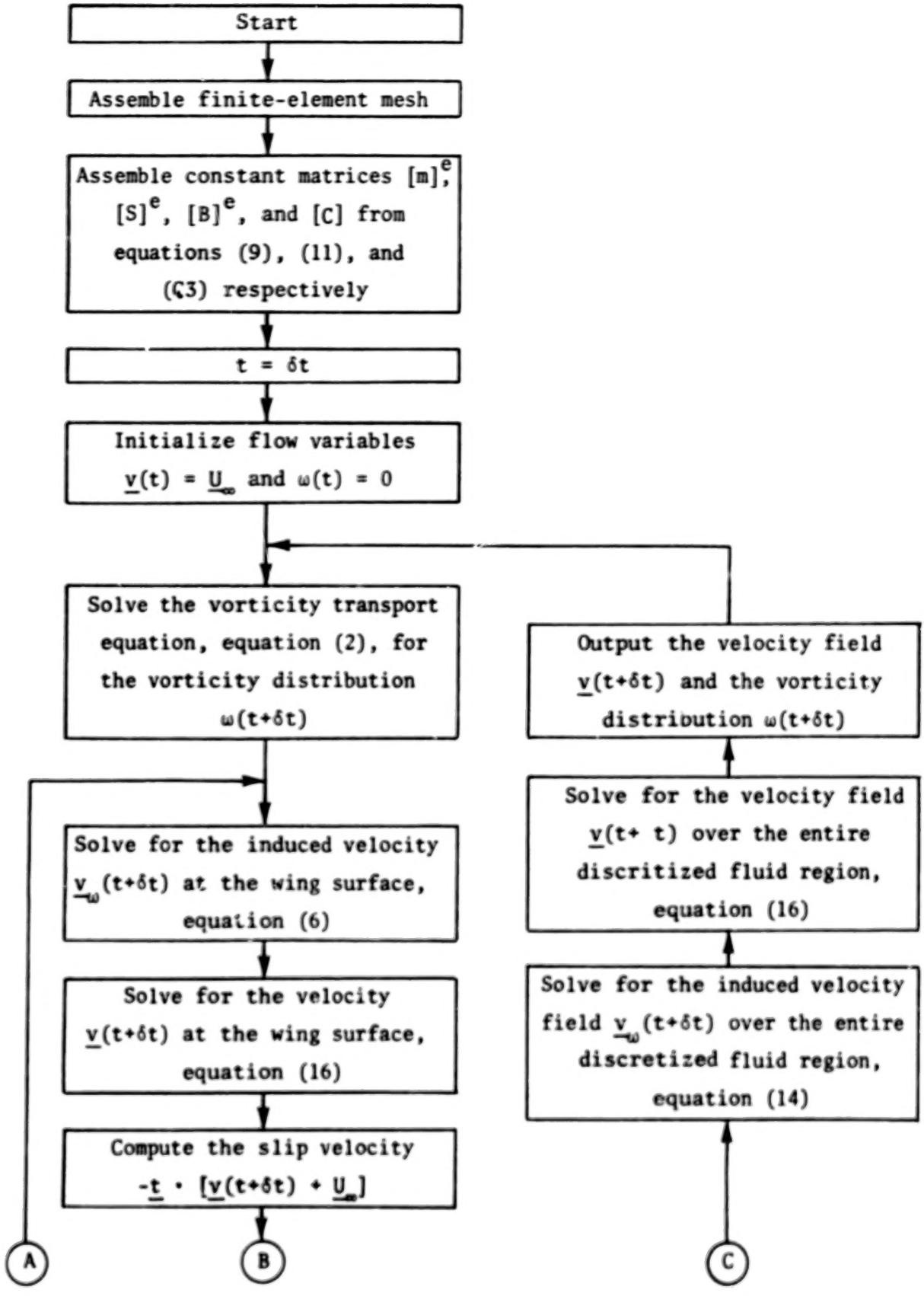
Start
Assemble finite-element mesh
Assemble constant matrices $[m]^e$, $[S]^e$, $[B]^e$, and [C] from equations (9), (11), and (C3) respectively
$t = \delta t$
Initialize flow variables $\underline{v}(t) = \underline{U}_\infty$ and $\omega(t) = 0$
Solve the vorticity transport equation, equation (2), for the vorticity distribution $\omega(t+\delta t)$
Solve for the induced velocity $\underline{v}_\omega(t+\delta t)$ at the wing surface, equation (6)
Solve for the velocity $\underline{v}(t+\delta t)$ at the wing surface, equation (16)
Compute the slip velocity $-\underline{t} \cdot [\underline{v}(t+\delta t) + \underline{U}_\infty]$
A
B
Output the velocity field $\underline{v}(t+\delta t)$ and the vorticity distribution $\omega(t+\delta t)$
Solve for the velocity field $\underline{v}(t+\delta t)$ over the entire discritized fluid region, equation (16)
Solve for the induced velocity field $\underline{v}_\omega(t+\delta t)$ over the entire discretized fluid region, equation (14)
C

Figure 1. The main sequence of computations in the computational procedure.

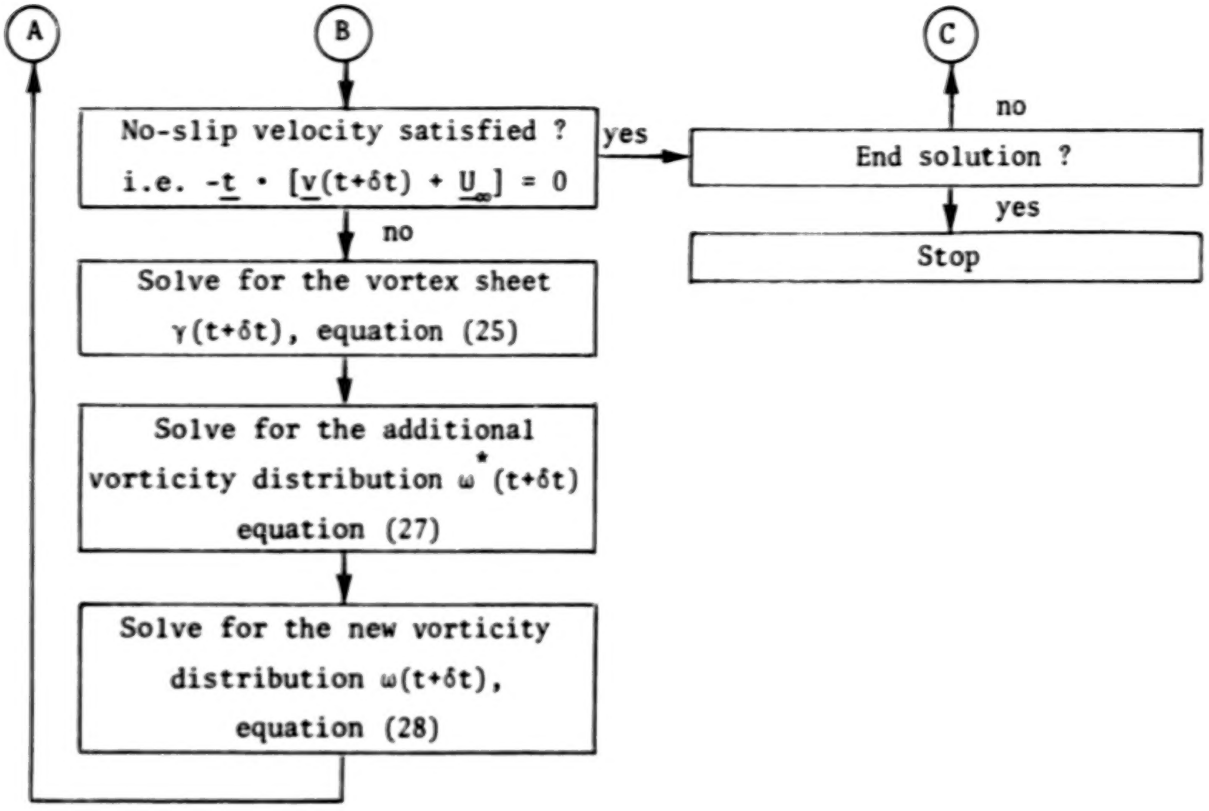

Figure 1. Concluded.

APPENDIX A

The Vorticity Transport Equations

The vorticity transport equations are discretized in space employing the finite-element method. Element equations are defined from a functional and then assembled to form a matrix-system of first-order differential equations. This system governs the fluid region. Using the method of weighted residuals, a statement for the vorticity transport equations can be written as

$$\int_A W \left\{ \frac{\partial \omega}{\partial t} + u \frac{\partial \omega}{\partial x} + v \frac{\partial \omega}{\partial y} - \nu \left(\frac{\partial^2 \omega}{\partial x^2} + \frac{\partial^2 \omega}{\partial y^2} \right) \right\} dA = 0 \qquad \text{(A1)}$$

The function W is approximated as

$$W = \sum_{k=1}^{m} M^k \omega_*^k \qquad \text{(A2)}$$

where the ω_*^k are arbitrary parameters and the M^k are weighting functions. On substitution of equation (A2) into equation (A1), the statement becomes

$$\int_A \sum_{k=1}^{m} M^k \omega_*^k \left\{ \frac{\partial \omega}{\partial t} + u \frac{\partial \omega}{\partial x} + v \frac{\partial \omega}{\partial y} - \nu \left\{ \frac{\partial^2 \omega}{\partial x^2} + \frac{\partial^2 \omega}{\partial y^2} \right\} \right\} dA = 0 \qquad \text{(A3)}$$

Since the parameters ω_*^k are arbitrary

$$\int_A \sum_{k=1}^{m} M^k \left\{ \frac{\partial \omega}{\partial t} + u \frac{\partial \omega}{\partial x} + v \frac{\partial \omega}{\partial y} - \nu \left\{ \frac{\partial^2 \omega}{\partial x^2} + \frac{\partial^2 \omega}{\partial y^2} \right\} \right\} dA = 0 \qquad \text{(A4)}$$

In equation (A4), the highest order derivatives are the second-order terms multiplied by ν, the viscous terms. Taking only the viscous terms from equation (A4) and applying a transformation by integration by parts (ref. 5) results in

$$- \nu \int_A M^k \left\{ \frac{\partial^2 \omega}{\partial x^2} + \frac{\partial^2 \omega}{\partial y^2} \right\} dA = - \nu \oint_c M^k \frac{\partial \omega}{\partial n} dc + \nu \int_A \left\{ \frac{\partial M^k}{\partial x} \frac{\partial \omega}{\partial x} + \frac{\partial M^k}{\partial y} \frac{\partial \omega}{\partial y} \right\} dA \qquad \text{(A5)}$$

On substitution of equation (A5) back into equation (A4), the statement for the vorticity transport equations becomes

$$\int_A \sum_{k=1}^{m} \left[M^k \left\{ \frac{\partial \omega}{\partial t} + u \frac{\partial \omega}{\partial x} + v \frac{\partial \omega}{\partial y} \right\} + \nu \left\{ \frac{\partial M^k}{\partial x} \frac{\partial \omega}{\partial x} + \frac{\partial M^k}{\partial y} \frac{\partial \omega}{\partial y} \right\} \right] dA \tag{A6}$$

$$- \nu \oint_c \sum_{k=1}^{m} M^k \frac{\partial \omega}{\partial n} dc = 0$$

where the highest order derivatives are now of the first-order. Applying the Galerkin process to equation (A6), the weighting functions M^k are set equal to the finite-element shape functions N_i.

The first space derivatives of the vorticity are determined from equations (E13) as follows

$$\frac{\partial \omega(\xi,\eta)}{\partial x} = \sum_{i=1}^{m} \frac{\partial N_i(\xi,\eta)}{\partial x} \omega_i = \{N_x\}^t \{\omega\}^e \tag{A7}$$

and

$$\frac{\partial \omega(\xi,\eta)}{\partial y} = \sum_{i=1}^{m} \frac{\partial N_i(\xi,\eta)}{\partial y} \omega_i = \{N_y\}^t \{\omega\}^e \tag{A8}$$

Similarly, the vorticity time-derivative is written as

$$\frac{\partial \omega(\xi,\eta)}{\partial t} = \sum_{i=1}^{m} N_i(\xi,\eta) \frac{\partial \omega_i}{\partial t} = \{N\}^t \frac{\partial \{\omega\}^e}{\partial t} \tag{A9}$$

Substitution of equations (A7-A9) and equations (E13-E15) into equation (A6) results in a matrix-system of differential equations over one finite-element as

$$[m]^e \frac{\partial \{\omega\}^e}{\partial t} = [A]^e \{\omega\}^e + [S]^e \{\omega\}^e + \{B\}^e \tag{A10}$$

The element mass matrix $[m]^e$ is given as

$$[m]^e = \int_A \{N\}\{N\}^t dA \tag{A11}$$

and the element convection and diffusion matrices are given as

$$[A]^e = - \int_A [\{N\}\{u\}^t\{N\}\{N_x\}^t + \{N\}\{v\}^t\{N\}\{N_y\}^t] \, dA \tag{A12}$$

$$[S]^e = - \nu \int_A [\{N_x\}\{N_x\}^t + \{N_y\}\{N_y\}^t] \, dA \tag{A13}$$

respectively. The element vector $\{B\}^e$ contains the wing vorticity boundary conditions

$$\{B\}^e = \nu \oint_c \{N\} \frac{\partial\{\omega\}}{\partial n} \, dc \tag{A14}$$

The integration of equations (A11-A14) being very difficult, it is therefore replaced by a numerical integration procedure as follows

$$\int_A f(x,y) \, dA = \sum_{k=1}^{g} f(\xi_k,\eta_k) \, w(\xi_k,\eta_k) \tag{A15}$$

Here the terms $w(\xi_k,\eta_k)$ are the integration weights corresponding to the total number of g integration points ξ_k,η_k. The integration over a finite-element is carried out in the local coordinate system of the finite-element. To transform a region to the one in which the integration is carried out, i.e., from the x,y plane to the ξ,η plane

$$dA = dxdy = \det[J] \, d\xi d\eta \tag{A16}$$

The finite-element matrices of equations (A11-A14) are thus numerically evaluated as

$$[m]^e = \sum_{k=1}^{g} \{N(\xi_k,\eta_k)\}\{N(\xi_k,\eta_k)\}^t \text{ det. } [J(\xi_k,\eta_k)] \, w(\xi_k,\eta_k) \tag{A17}$$

$$[A]^e = - \sum_{k=1}^{g} \{\{N(\xi_k,\eta_k)\}\{u\}^t\{N(\xi_k,\eta_k)\}^t\{N_x(\xi_k,\eta_k)\}^t + \{N(\xi_k,\eta_k)\}\{v\}^t\{N(\xi_k,\eta_k)\}^t\{N_y(\xi_k,\eta_k)\}^t\} \text{ det. } [J(\xi_k,\eta_k)] \, w(\xi_k,\eta_k) \tag{A18}$$

$$[S]^e = -\nu \sum_{k=1}^{g} \{\{N_x(\xi_k,\eta_k)\}\{N_x(\xi_k,\eta_k)\}^t + \{N_y(\xi_k,\eta_k)\}\{N_y(\xi_k,\eta_k)\}^t\} [J(\xi_k,\eta_k)]\, w(\xi_k,\eta_k) \tag{A19}$$

and

$$[B]^e = \nu \sum_{k=1}^{g} \{N(\xi_k,-1)\}\{N_\eta(\xi_k,-1)\}^t [J(\xi_k,-1)]\, w(\xi_k) \{\omega\} \tag{A20}$$

respectively. In equation (A20) the integration is over the side of the finite-element in contact with the wing surface. For the quadrilateral finite-element this side corresponds to $\eta = -1$ (see figure E.2). The derivatives in the Cartesian coordinate system of the element shape functions are obtained in terms of their local derivative with equation (E5).

The element equations are now assembled to form a global matrix-system of equations, which governs the fluid region as

$$[m] \frac{\partial\{\omega\}}{\partial t} = [A]\{\omega\} + [S]\{\omega\} + [B]\{\omega\} \tag{A21}$$

Equation (A21) is then solved in time using a finite-difference technique to obtain a new distribution of vorticity.

APPENDIX B

The Velocity Field

The velocity field $\underline{v}(t+\delta t)$ of the fluid region is defined in general as

$$\underline{v}(t+\delta t) = \underline{v}_{\omega}(t+\delta t) + \underline{U}_{\infty} \tag{B1}$$

The induced velocity $\underline{v}_{\omega}(t+\delta t)$ is given by the Biot-Savart law. It is due to the vorticity distribution $\omega(t+\delta t)$ in the fluid region. The velocity $\underline{U}_{\infty}$ is the onset velocity. It is constant in space and time. Defined by their values at all finite-element nodes in the fluid region, the velocity components at a finite-element node i are given as

$$\begin{aligned} u^i(t+\delta t) &= u_{\infty} + u^i_{\omega}(t+\delta t) \\ v^i(t+\delta t) &= v_{\infty} + v^i_{\omega}(t+\delta t) \end{aligned} \tag{B2}$$

Each finite-element will contribute toward the induced velocity at a finite-element node i due to the vorticity distribution over it. For finite-element A_j, the contributions to the induced velocity components are obtained as

$$u^i_{\omega}(t+\delta t) = -\frac{1}{2\pi}\int_{A_j} \frac{\omega_j(t+\delta t)(y_i-y_j)}{|\underline{r}_{ij}|^2}\, dA_j \tag{B3}$$

and

$$v^i_{\omega}(t+\delta t) = +\frac{1}{2\pi}\int_{A_j} \frac{\omega_j(t+\delta t)(x_i-x_j)}{|\underline{r}_{ij}|^2}\, dA_j \tag{B4}$$

with

$$|\underline{r}_{ij}|^2 = (x_i-x_j)^2 + (y_i-y_j)^2 \tag{B5}$$

The individual velocity components are summed over all finite-elements (f.e.) to give the complete induced velocity at node i as

$$\underline{v}^i_{\omega}(t+\delta t) = \sum^{f.e.} u^i_{\omega}(t+\delta t)\underline{i} + \sum^{f.e.} v^i_{\omega}(t+\delta t)\underline{j} \tag{B6}$$

The integrals of equations (B3) and (B4) are integrated numerically, using equations (A15) and (A16), as follows

$$u_{\omega}^{i}(t+\delta t) = -\frac{1}{2\pi} \sum_{k=1}^{g} \frac{\omega(\xi_k,\eta_k)\ \{y_i - y(\xi_k,\eta_k)\}}{|\underline{r}_{ik}|^2} \det.\ [J(\xi_k,\eta_k)]\ w(\xi_k,\eta_k) \quad (B7)$$

and

$$v_{\omega}^{i}(t+\delta t) = +\frac{1}{2\pi} \sum_{k=1}^{g} \frac{\omega(\xi_k,\eta_k)\ \{x_i - x(\xi_k,\eta_k)\}}{|\underline{r}_{ik}|^2} \det.\ [J(\xi_k,\eta_k)]\ w(\xi_k,\eta_k) \quad (B8)$$

The vorticity $\omega(\xi_k,\eta_k)$ and the coordinates $x(\xi_k,\eta_k)$ and $y(\xi_k,\eta_k)$ are obtained from equations (E1), (E2), and (E13). For the quadrilateral finite-element and the triangular finite-element, the terms of the Jacobian [J] are computed from equations (E7) and (E11) respectively.

APPENDIX C

The Vortex Sheet

The vortex sheet is determined using a numerical technique developed by Hess and Smith (ref. 16) and which was refined by Argyris and Scharpf (ref. 17). Collecting the nodal values γ of the vortex sheet intensity into the vector $\{\gamma\}$, equation (25) may be written in matrix form as

$$[C]\{\gamma\} = \{F\} \tag{C1}$$

Solving equation (C1) for the unknown vector $\{\gamma\}$ results in

$$\{\gamma\} = [C]^{-1}\{F\} \tag{C2}$$

The manner in which the terms of the coefficient matrix [C] are determined is now summarized. Equation (25) is applied to one of the curvilinear element-nodes and is then integrated around the wing-contour c. The integration around the contour c is accomplished by integrating over segments of contour c, defined by the curvilinear elements and then summing their contributions. For node i and curvilinear element c_k the terms of matrix [C] are given as

$$C_{ij} = \frac{L_j(x_i,y_i)}{2} + \underline{t}_i \cdot \frac{1}{2\pi}\,\underline{S} \tag{C3}$$

where the components of the vector $\underline{S}$ are given as

$$S_x = -\int_{c_k} \frac{L_j(x_k,y_k)\,(y_i - y_k)}{|\underline{r}_{ik}|^2}\,dc_k \tag{C4}$$

and

$$S_y = +\int_{c_k} \frac{L_j(x_k,y_k)\,(x_i - x_k)}{|\underline{r}_{ik}|^2}\,dc_k \tag{C5}$$

Here the parameters L_j are the Lagrangian interpolation polynomials of equations (D8). They define a vortex sheet of unit intensity over curvilinear element c_k. The position vector $\underline{r}_{ik}$ is given as

$$|\underline{r}_{ik}|^2 = (x_i - x_k)^2 + (y_i - y_k)^2 \tag{C6}$$

The terms of the vector $\{F\}$, on the right-hand side of equation (C1), are determined as

$$F_i = - \underline{t}_i \cdot (\underline{U}_\infty + \underline{v}_\omega)_i \tag{C7}$$

The induced velocity $\underline{v}_\omega$ is obtained from equations (B7) and (B8). Equations (C4) and (C5) are integrated numerically as follows

$$S_x = - \sum_{k=1}^{g} \frac{L_j(\xi_k)\{y_i - y(\xi_k)\}}{|\underline{r}_{ik}|^2} \{x_{,\xi_k}^2 + y_{,\xi_k}^2\}^{\frac{1}{2}} w_k \tag{C8}$$

and

$$S_y = + \sum_{k=1}^{g} \frac{L_j(\xi_k)\{x_i - x(\xi_k)\}}{|\underline{r}_{ik}|^2} \{x_{,\xi_k}^2 + y_{,\xi_k}^2\}^{\frac{1}{2}} w_k \tag{C9}$$

Here, the parameters ξ_k are the local coordinates of the integration points with weights w_k. The derivatives of the Cartesian coordinates with respect to the local coordinate (ξ,η) are found from equation (D6).

APPENDIX D

Representation of the Wing Boundary

The wing contour c is divided into a series of curvilinear line-elements according to Arygris and Scharpf (ref. 17). A Hermitian interpolation model is used to describe the geometry of each curvilinear element. A Lagrangian interpolation model is used to describe the vortex sheet intensity over each element. Figure D.1 illustrates a single curvilinear element with the vortex sheet of intensity γ acting over it. Each element is defined by three nodes.

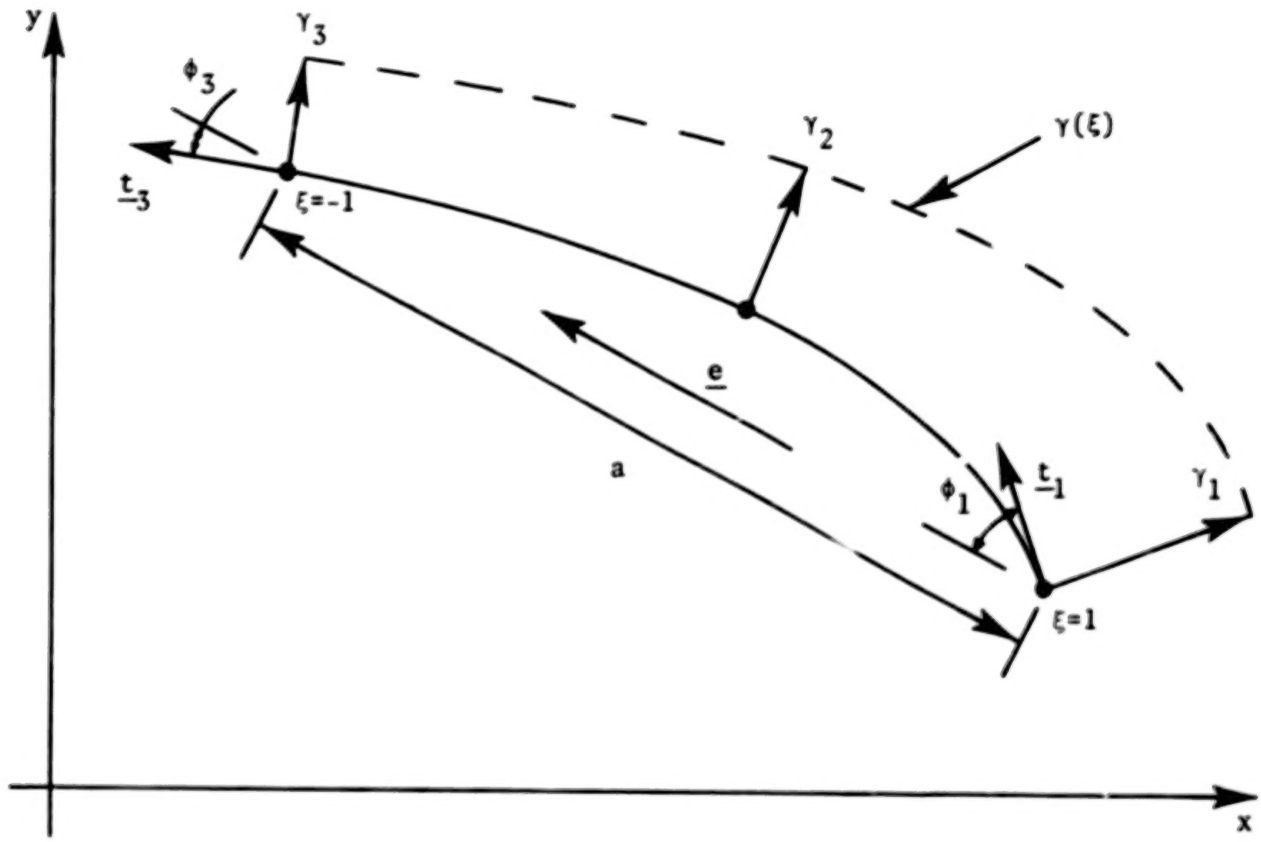

Figure D.1 The curvilinear element after Argyris and Scharpf (ref. 17).

The geometry of a curvilinear element is defined by the known Cartesian coordinates of the element end-nodes and the prescribed tangential directions at those nodes. The Hermitian polynomials used are

$$H_1 = \frac{1}{4}\left(2 + 3\xi - \xi^3 \right)$$

$$H_2 = \frac{1}{4}\left(-1 + \xi + \xi^2 - \xi^3 \right) \qquad \text{(D1)}$$

$$H_3 = \frac{1}{4}\left(2 - 3\xi + \xi^3 \right)$$

$$H_4 = \frac{1}{4}\left(+1 + \xi - \xi^2 - \xi^3 \right) \qquad \text{(D1)}$$

Here ξ is a local coordinate defined over the curvilinear element ranging in value between -1 and +1.

A local coordinate point ξ is mapped into the (x,y) plane by

$$\begin{Bmatrix} x(\xi) \\ y(\xi) \end{Bmatrix} = \begin{Bmatrix} x_1 & x_{1,\xi} & x_3 & x_{3,\xi} \\ y_1 & y_{1,\xi} & y_3 & y_{3,\xi} \end{Bmatrix} \begin{bmatrix} H_1 \\ H_2 \\ H_3 \\ H_4 \end{bmatrix} \qquad \text{(D2)}$$

The measures of the derivatives of x or y with respect to ξ at the nodes of the element are given by

$$\left.\frac{dx}{d\xi}\right|_k = x_{k,\xi} = q_k\, t_x^k$$

$$\left.\frac{dy}{d\xi}\right|_k = y_{k,\xi} = q_k\, t_y^k \qquad \text{(D3)}$$

as suggested by Argyris and Scharpf (ref. 17). The parameter q_k is defined (ref. 17) as

$$q_k = \frac{a}{2}\,\frac{\phi_k}{\cos\,\phi_k} \qquad \text{(D4)}$$

and

$$\cos\,\phi_k = \underline{t}_k \cdot \underline{e} \qquad \text{(D5)}$$

For an arbitrary point on a curvilinear element, the derivatives of x or y with respect to ξ are written as

$$\begin{Bmatrix} x_{,\xi} \\ y_{,\xi} \end{Bmatrix} = \begin{Bmatrix} x_1 & x_{1,\xi} & x_3 & x_{3,\xi} \\ y_1 & y_{1,\xi} & y_3 & y_{3,\xi} \end{Bmatrix} \begin{bmatrix} H_{1,\xi} \\ H_{2,\xi} \\ H_{3,\xi} \\ H_{4,\xi} \end{bmatrix} \qquad \text{(D6)}$$

The derivatives of the Hermitian polynomials with respect to ξ are found from equations (D2).

The intensity of the vortex sheet over a curvilinear element is approximated using the Lagrangian interpolation polynomials L_i and the known intensity of the vortex sheet at the three nodes of the element. At an arbitrary point on the curvilinear element, the intensity of the vortex sheet is written as

$$\gamma(\xi) = \sum_{j=1}^{3} L_j(\xi)\gamma_j = \{L\}^t\{\gamma\}^e \tag{D7}$$

where the values of γ_i are the nodal values of the vortex sheet intensity. The Lagrangian polynomials used in equation (D7) are

$$L_1 = \frac{1}{2}\xi(\xi + 1)$$

$$L_2 = 1 - \xi^2 \tag{D8}$$

$$L_3 = \frac{1}{2}\xi(\xi - 1)$$

where ξ is the local coordinate defined over the element.

APPENDIX E

Representation of the Two-Dimensional Fluid Region

The two-dimensional fluid region A is represented by subdividing it into a finite number of finite-elements. A finite-element mesh is illustrated in figure E.1. The flow variables, vorticity ω and velocity $\underline{v}=(u,v)$, are sought at the nodes. Two types of finite-elements are used to divide the fluid region A: isoparametric quadrilateral finite-elements and isoparametric triangular finite-elements.

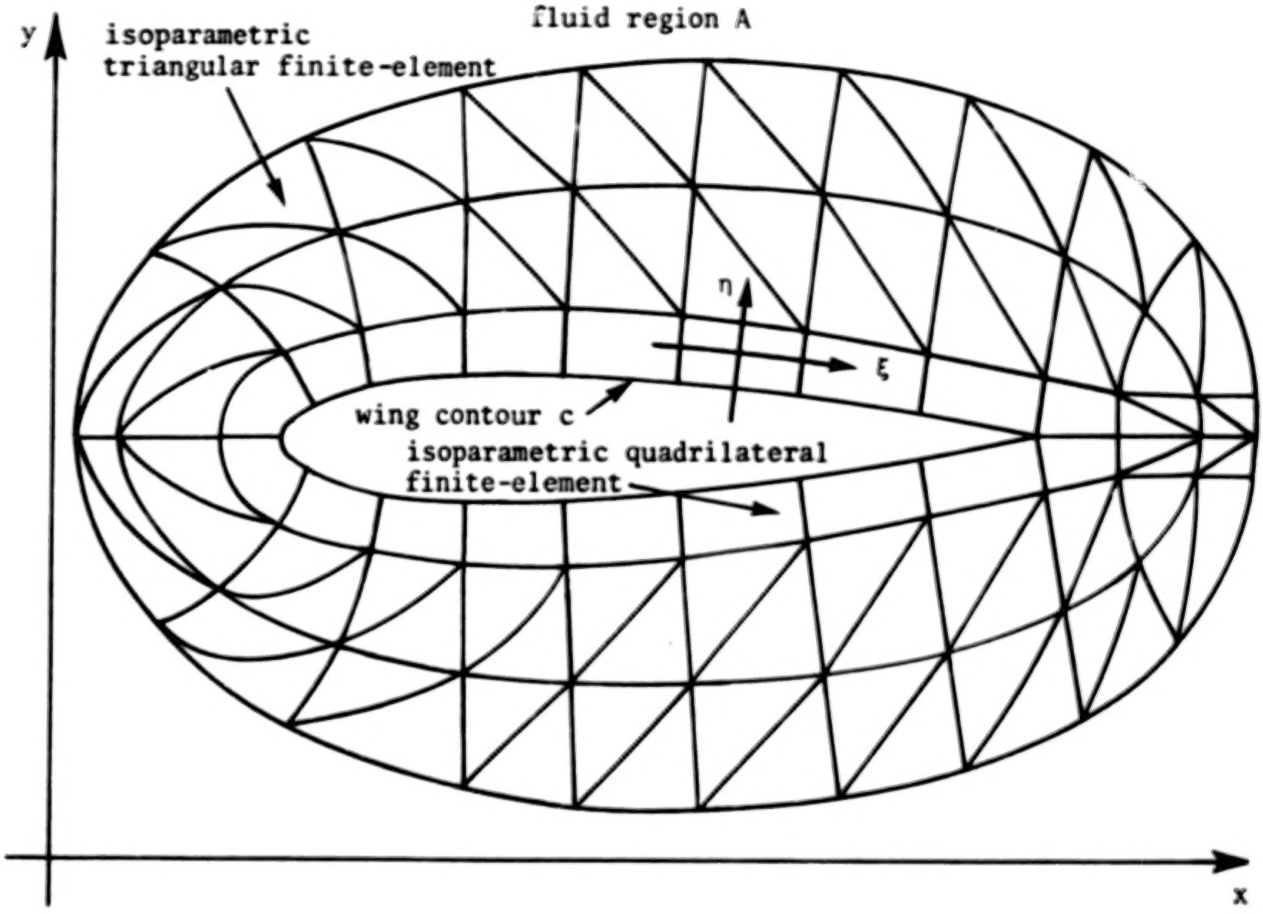

Figure E.1 Illustration of the finite-element mesh.

Isoparametric finite-elements better approximate the curved boundary of the wing. Considering the local coordinates (ξ,η) and the corresponding Cartesian coordinates (x,y), a point in the (ξ,η) plane is mapped into the corresponding point in the (x,y) plane by

$$x(\xi,\eta) = \sum_{i=1}^{m} N_i(\xi,\eta)x_i \qquad \text{(E1)}$$

and

$$y(\xi,\eta) = \sum_{i=1}^{m} N_i(\xi,\eta) y_i \tag{E2}$$

Here, the coordinates (x_i,y_i) are the known coordinates of the finite-element nodes. Each finite-element is defined by m nodes. The shape functions, N_i, are expressed in terms of the local coordinates (ξ,η) which range between unity and zero within the element. Local derivatives of the shape functions are expressed in terms of their Cartesian derivatives by the chain rule.

$$\begin{aligned} \frac{\partial N_i}{\partial \xi} &= \frac{\partial N_i}{\partial x}\frac{\partial x}{\partial \xi} + \frac{\partial N_i}{\partial y}\frac{\partial y}{\partial \xi} \\ \frac{\partial N_i}{\partial \eta} &= \frac{\partial N_i}{\partial x}\frac{\partial x}{\partial \eta} + \frac{\partial N_i}{\partial y}\frac{\partial y}{\partial \eta} \end{aligned} \tag{E3}$$

or in matrix form

$$\begin{bmatrix} \frac{\partial N_i}{\partial \xi} \\ \frac{\partial N_i}{\partial \eta} \end{bmatrix} = \begin{bmatrix} \frac{\partial x}{\partial \xi} & \frac{\partial y}{\partial \xi} \\ \frac{\partial x}{\partial \eta} & \frac{\partial y}{\partial \eta} \end{bmatrix} \begin{bmatrix} \frac{\partial N_i}{\partial x} \\ \frac{\partial N_i}{\partial y} \end{bmatrix} = [J] \begin{bmatrix} \frac{\partial N_i}{\partial x} \\ \frac{\partial N_i}{\partial y} \end{bmatrix} \tag{E4}$$

where [J] is the Jacobian. The Cartesian derivatives of the shape functions can then be found in terms of their local derivatives as

$$\begin{bmatrix} \frac{\partial N_i}{\partial x} \\ \frac{\partial N_i}{\partial y} \end{bmatrix} = [J]^{-1} \begin{bmatrix} \frac{\partial N_i}{\partial \xi} \\ \frac{\partial N_i}{\partial \eta} \end{bmatrix} \tag{E5}$$

Figure E.2 illustrates the isoparametric quadrilateral finite-element.

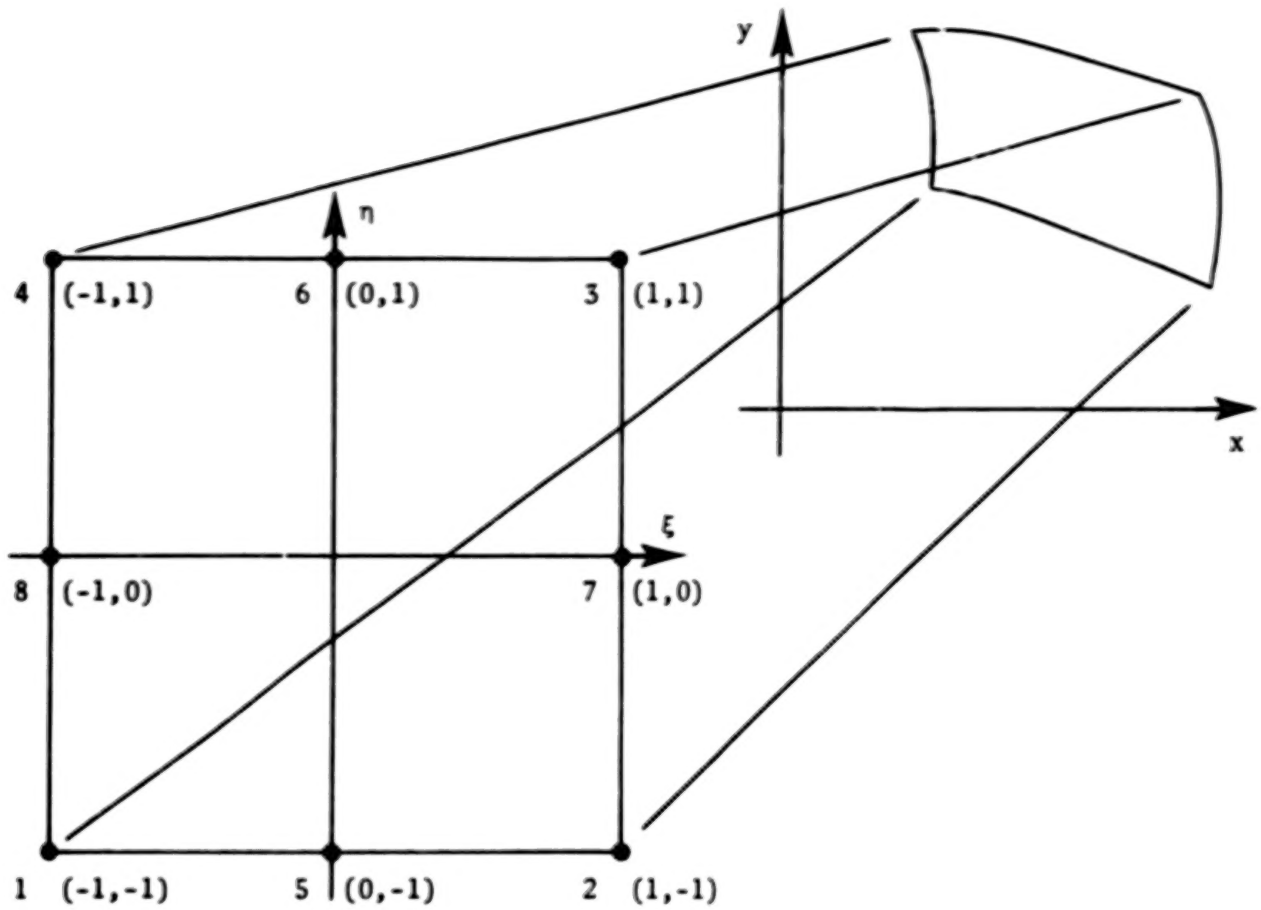

Figure E.2 The isoparametric quadrilateral finite-element.

The shape functions used for quadrilateral finite-element geometry are

$$N_1 = \frac{1}{4}\left(-1 + \xi^2 - \xi^2\eta + \xi\eta - \xi\eta^2 + \eta^2 \right)$$

$$N_2 = \frac{1}{4}\left(-1 + \xi^2 - \xi^2\eta - \xi\eta + \xi\eta^2 + \eta^2 \right)$$

$$N_3 = \frac{1}{4}\left(-1 + \xi^2 + \xi^2\eta + \xi\eta + \xi\eta^2 + \eta^2 \right)$$

$$N_4 = \frac{1}{4}\left(-1 + \xi^2 + \xi^2\eta - \xi\eta - \xi\eta^2 + \eta^2 \right) \qquad \text{(E6)}$$

$$N_5 = \frac{1}{2}\left(1 - \xi^2 + \xi^2\eta - \eta \right)$$

$$N_6 = \frac{1}{2}\left(1 - \xi^2 - \xi^2\eta + \eta \right)$$

$$N_7 = \frac{1}{2}\left(1 + \xi - \xi\eta^2 - \eta^2 \right)$$

$$N_8 = \frac{1}{2}\left(1 - \xi + \xi\eta^2 - \eta^2 \right) \tag{E6}$$

Using equations (E1) and (E2), the elements of the Jacobian for the quadrilateral element may be written as

$$\frac{\partial x}{\partial \xi} = \sum_{i=1}^{8} \frac{\partial N_i}{\partial \xi} x_i \qquad \frac{\partial y}{\partial \xi} = \sum_{i=1}^{8} \frac{\partial N_i}{\partial \xi} y_i$$

$$\frac{\partial x}{\partial \eta} = \sum_{i=1}^{8} \frac{\partial N_i}{\partial \eta} x_i \qquad \frac{\partial x}{\partial \eta} = \sum_{i=1}^{8} \frac{\partial N_i}{\partial \eta} y_i \tag{E7}$$

The derivative of the shape functions with respect to the local coordinates is computed directly from equation (E6).

The isoparametric triangular finite-element is illustrated in figure E.3. Local coordinates, used for the triangular finite-element, are the area coordinates (ℓ_1,ℓ_2,ℓ_3) corresponding to the Cartesian coordinate point (x,y). The applied shape functions are quadratic. The corner nodes are

$$\begin{aligned} N_1 &= \ell_1 (2\ell_1 - 1) \\ N_2 &= \ell_2 (2\ell_2 - 1) \\ N_3 &= \ell_3 (2\ell_3 - 1) \end{aligned} \tag{E8}$$

and the mid-side nodes

$$\begin{aligned} N_4 &= 4\ell_1\ell_2 \\ N_5 &= 4\ell_2\ell_3 \\ N_6 &= 4\ell_3\ell_1 \end{aligned} \tag{E9}$$

The Cartesian derivatives for the triangular finite-element shape functions are expressed in terms of their local derivatives. Letting

$$\xi = \ell_1 \qquad \eta = \ell_2 \qquad 1 - \xi - \eta = \ell_3 \tag{E10}$$

then by the chain rule

$$
\begin{aligned}
\frac{\partial x}{\partial \xi} &= \frac{\partial x}{\partial \ell_1}\frac{\partial \ell_1}{\partial \xi} + \frac{\partial x}{\partial \ell_2}\frac{\partial \ell_2}{\partial \xi} + \frac{\partial x}{\partial \ell_3}\frac{\partial \ell_3}{\partial \xi} \\
\frac{\partial x}{\partial \eta} &= \frac{\partial x}{\partial \ell_1}\frac{\partial \ell_1}{\partial \eta} + \frac{\partial x}{\partial \ell_2}\frac{\partial \ell_2}{\partial \eta} + \frac{\partial x}{\partial \ell_3}\frac{\partial \ell_3}{\partial \eta} \\
\frac{\partial y}{\partial \xi} &= \frac{\partial y}{\partial \ell_1}\frac{\partial \ell_1}{\partial \xi} + \frac{\partial y}{\partial \ell_2}\frac{\partial \ell_2}{\partial \xi} + \frac{\partial y}{\partial \ell_3}\frac{\partial \ell_3}{\partial \xi} \\
\frac{\partial y}{\partial \eta} &= \frac{\partial y}{\partial \ell_1}\frac{\partial \ell_1}{\partial \eta} + \frac{\partial y}{\partial \ell_2}\frac{\partial \ell_2}{\partial \eta} + \frac{\partial y}{\partial \ell_3}\frac{\partial \ell_3}{\partial \eta}
\end{aligned}
\qquad \text{(E11)}
$$

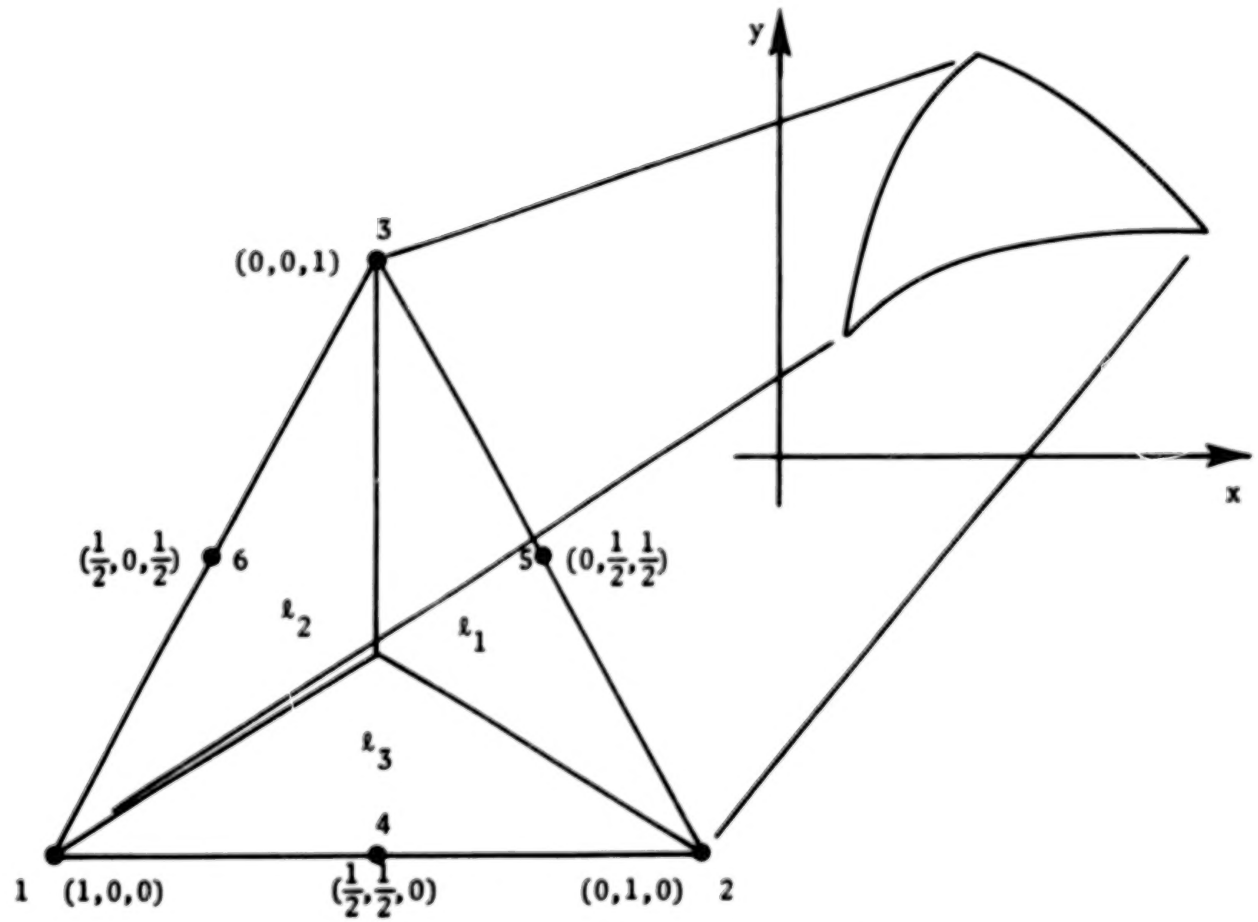

Figure E.3 The isoparametric triangular finite-element.

Using equations (E10), the terms of the Jacobian are found from equations (E11) as

$$\frac{\partial x}{\partial \xi} = \frac{\partial x}{\partial \ell_1} - \frac{\partial x}{\partial \ell_3} \qquad \frac{\partial y}{\partial \xi} = \frac{\partial y}{\partial \ell_1} - \frac{\partial y}{\partial \ell_3}$$

$$\frac{\partial x}{\partial \eta} = \frac{\partial x}{\partial \ell_2} - \frac{\partial x}{\partial \ell_3} \qquad \frac{\partial y}{\partial \eta} = \frac{\partial y}{\partial \ell_2} - \frac{\partial y}{\partial \ell_3} \tag{E12}$$

The remaining derivatives of the coordinates (x,y) on the right-hand side of equation (E12) are found in terms of the area coordinates (ℓ_1,ℓ_2,ℓ_3) using equations (E1) and (E2).

Over each finite-element, the vorticity and velocity components are approximated by their nodal values ω_i, u_i, and v_i and the nodal shape functions N_i. Then

$$\omega(\xi,\eta) = \sum_{i=1}^{m} N_i(\xi,\eta)\omega_i = \{N\}^t\{\omega\}^e \tag{E13}$$

and

$$u(\xi,\eta) = \sum_{i=1}^{m} N_i(\xi,\eta)u_i = \{N\}^t\{u\}^e \tag{E14}$$

$$v(\xi,\eta) = \sum_{i=1}^{m} N_i(\xi,\eta)v_i = \{N\}^t\{v\}^e \tag{E15}$$

The super-script e indicates an element vector or matrix.

REFERENCES

1. McCroskey, W.J.: Some Current Research in Unsteady Fluid Dynamics. Trans. of ASME, J. of Fluids Eng. vol. 99, no. 3, 1977, pp. 8-38.

2. White, F.M.: Viscous Fluid Flow. McGraw-Hill Book Co., 1974.

3. Bratanow, T.; and Spehert, T.: Recent Findings on the Inclusion of Vorticity in the Numerical Analysis of Unsteady High Reynolds Number Flows. Int. Conf. on Applied Numerical Modelling, Univ. of Southampton, Southampton, England, 11-15 July, 1977.

4. Norrie, D.H.; and de Vries, G.: A Survey of the Finite Element Applications in Fluid Mechanics. Rep. No. 83, Mech. Eng. Dept., Univ. of Calgary, Calgary, Alberta, Canada, Dec., 1976.

5. Zienkiewicz, O.C.: The Finite Element Method in Engineering Science. Second ed. McGraw-Hill Publishing Co., Ltd., London, England, 1971.

6. Huebner, K.H.: The Finite Element Method for Engineers. John Wiley and Sons, Inc., 1975.

7. Lighthill, M.J.: Introduction. Boundary Layer Theory. Laminar Boundary Layers. Chapter II, L. Rosenhead, ed., Oxford University Press, Oxford, England, 1963, pp. 46-113.

8. Payne, R.B.: Calculations of Unsteady Viscous Flow Past a Circular Cylinder. J. Fluid Mech., vol. 4, 1958, pp. 81-86.

9. Schmall, R.A.; and Kinney, R.B.: Numerical Study of Unsteady Viscous Flow Past a Lifting Plate. AIAA J., vol. 12, no. 11, 1974, pp. 1566-1573.

10. Wu, J.C.: Numerical Boundary Conditions for Viscous Flow Problems. AIAA J., vol. 14, no. 8, 1976, pp. 1042-1049.

11. Wu, J.C.; and Thompson, J.F.: Numerical Solution of Time-Dependent Incompressible Navier-Stokes Equations Using an Integro-Differential Formulation. J. Computers and Fluids, vol. 1, no. 2, 1973, pp. 197-215.

12. Schlichting, H.: Boundary Layer Theory. Sixth ed., McGraw-Hill Book Co., 1968.

13. Whitham, G.B.: The Navier-Stokes Equations of Motion. Laminar Boundary Layers. Chapter III, L. Rosenhead, ed., Oxford University Press, Oxford, England, 1963, pp. 114-128.

14. Roache, P.J.: Computational Fluid Dynamics. Hermosa Publishers, 1972.

15. Hunt, J.N.: Incompressible Fluid Dynamics. American Elsevier Publishing Co., Inc., 1965.

16. Hess, J.L.; and Smith, A.M.O.: Calculation of Potential Flow about Arbitrary Bodies. Prog. in Aeronautical Science, Pergamon Press, vol. 8, 1967, pp. 1-138.

17. Argyris, J.H.; and Scharpf, D.W.: Two and Three-dimensional Potential Flow by the Method of Singularities. J. Roy. Aeronaut. Soc., vol. 73, no. 11, 1969, pp. 959-961.

18. Milne-Thomson, L.M.: Theoretical Aerodynamics. Fourth ed. Dover Publications, Inc., 1958.

19. Milne-Thomson, L.M.: Theoretical Hydrodynamics. Fifth ed. Macmillan Co., 1968.

1. Report No.	2. Government Accession No.	3. Recipient's Catalog No.
NASA CR-2995		

4. Title and Subtitle	5. Report Date
COMPUTATIONAL FLOW DEVELOPMENT FOR UNSTEADY VISCOUS FLOWS - Foundation of the Numerical Method	May 1978
	6. Performing Organization Code
7. Author(s)	8. Performing Organization Report No.
Theodore Bratanow and Thomas Spehert	
	10. Work Unit No.
9. Performing Organization Name and Address	11. Contract or Grant No.
University of Wisconsin-Milwaukee Milwaukee, Wisconsin 53201	NGR-50-007-001
	13. Type of Report and Period Covered
12. Sponsoring Agency Name and Address	Contractor Report
National Aeronautics and Space Administration Washington, D.C. 20546	14. Sponsoring Agency Code

15. Supplementary Notes

Langley Technical Monitor: Warren H. Young, Jr.

Progress Report

16. Abstract

A procedure is presented for effective consideration of viscous effects in computational development of high Reynolds number flows. The procedure is based on the interpretation of the Navier-Stokes equations as vorticity transport equations. The physics of the flow has been represented in a form suitable for numerical analysis. Lighthill's concept for flow development for computational purposes has been adapted. The vorticity transport equations were cast in a form convenient for computation. A statement for these equations was written using the method of weighted residuals and applying the Galerkin criterion. An integral representation of the induced velocity was applied on the basis of the Biot-Savart law. The numerical procedure developed by Hess and Smith and then refined by Argyris and Scharpf was used in computing vortex sheets over curved wing surfaces. Distribution of new vorticity, produced at wing surfaces over small computational time intervals was assumed to be confined to a thin region around the wing surfaces. This report presents thus the foundation and components of the numerical method. A following report will present the details of the implementation of the computational procedure.

17. Key Words (Suggested by Author(s))	18. Distribution Statement
FINITE-ELEMENT ANALYSIS NAVIER-STOKES EQUATIONS UNSTEADY FLOW COMPUTATIONAL FLOW DEVELOPMENT	UNCLASSIFIED - UNLIMITED Subject Category 34

19. Security Classif. (of this report)	20. Security Classif. (of this page)	21. No. of Pages	22. Price*
UNCLASSIFIED	UNCLASSIFIED	37	$4.50

* For sale by the National Technical Information Service, Springfield, Virginia 22161

NASA-Langley, 1978

END

9. 19. 78